Erschienen in: SiliconPV 2019, The 9th International Conference on Crystalline Silicon Photovoltaics : 8-10 April 2019, Leuven, Belgium / Poortmans, Jef et al. (Hrsg.). - Melville, New York : AIP Publishing, 2019. - (AIP Conference Proceedings ; 2147,1). - 020015. - ISBN 978-0-7354-1892-9
http://dx.doi.org/10.1063/1.5123820

Injection Resolved Spatial Lifetime Mapping using Photoluminescence

Daniel Skorka[1,a)], Annika Zuschlag[1,b)] and Giso Hahn[1,c)]

[1]*Department of Physics, University of Konstanz, Universitätsstraße 10, 78457 Konstanz, Germany*

[a)]Corresponding author: daniel.skorka@uni-konstanz.de
[b)]annika.zuschlag@uni-konstanz.de
[c)]giso.hahn@uni-konstanz.de

Abstract. The excess minority charge carrier lifetime τ_{eff} is an important metric for the performance of silicon based photovoltaic devices. In addition, its dependence on excess charge carrier concentration Δn can be used to identify defects and defect configurations. In multicrystalline (mc) silicon materials with strong local variations in quality and contamination, this dependence needs to be known with spatial resolution. Even in high quality Floatzone silicon (FZ-Si) wafers localized defects may exist. In this work, we employ Time Resolved PhotoLuminescence Imaging (TR-PLI) to obtain spatially resolved lifetime maps of silicon wafers passivated with aluminum oxide at different levels of excitation with light. Using this data, we determine the spatially resolved injection dependence for each pixel separately, without recourse to another method of lifetime measurement.

INTRODUCTION

With the continuing improvement in efficiencies of silicon based solar cells, the electronic quality of wafer material is becoming an ever more important topic. Detrimental effects include contamination with iron or oxygen, leading to phenomena called FeB and BO-LID (boron-oxygen light induced degradation) [1]. An as yet unexplained effect called LeTID (light and elevated temperature induced degradation) has first been observed in mc-Si [2,3], but has since been suspected to occur in both Czochralski silicon (Cz-Si) [4] and FZ-Si, too [5]. The latter material may also show areas of severely lower lifetime, depending on treatment [6,7].

Defects can be characterized and identified by their Shockley-Read-Hall parameters, describing the injection dependence of their recombination activity. Hence, the measurement of injection dependent lifetime of minority charge carriers $\tau(\Delta n)$ is an important method. Since inhomogeneities in either defect distribution (FeB), background wafer quality (mc-Si) or surface passivation layers are common, this should ideally be a measurement of $\tau(\Delta n, \vec{r})$.

The TR-PLI [8,9] method uses imaging to obtain a lifetime map of a wafer within minutes. However, a shortcoming of this method is that it obtains a single image at constant excitation. While this most closely reflects real operating conditions of the device under test, it is not sufficient for performing defect analysis. In this work, we present an extension of this method that allows to extract the spatially resolved, injection dependent minority charge carrier lifetime $\tau(\Delta n, \vec{r})$.

EXPERIMENTAL

Sample Preparation

In this study commercially available Boron-doped FZ-Si material with a resistivity of about 200 Ωcm was used. The wafer (150 mm round with flat, 250 µm thick, polished surfaces) was inscribed along the flat using a diamond

cutter tool and then processed as follows: After immersion in dilute HF for 1.5 min to remove any surface oxide, it was briefly rinsed in DI water and blow dried using N_2.

It was then deposited on both sides with ~15 nm of AlO_x at 170°C in a plasma-enhanced atomic layer deposition tool (Oxford Instruments ALD FlexAL MK2). Afterwards it was annealed in a dry N_2 atmosphere at a set temperature of 470 °C (sample temperature around 420 °C) for 20 min.

Measurement

A first measurement was performed using the PCD method [10,11] (Sinton Instruments WCT-120, transient mode, 1/64 flash), positioning the sample on the stage such that the flat was at the 70 mm mark.

Afterwards, an area of about 8x8 cm² of the sample centered on the same position as the PCD coil was imaged using TR-PLI. The sample was held in place above a glass plate and excited with an array of LEDs (λ_{max}= 630 nm) from below. The effective photon flux was varied in the range $1.3 \cdot 10^{16}$ – $1.3 \cdot 10^{17}$ $cm^{-2}s^{-1}$, and the illuminated area was substantially larger than the mapped area. Reflection from the surface was estimated to be 22 %, with total absorption of the remaining 78 %. At each photon flux, 25 TR-PLI acquisitions with 8 phase images each were performed and then averaged to reduce the effect of noise. Forced air cooling was used to keep the sample from heating up due to the unusually many and long acquisitions. The TR-PLI frequency used was either 1 or 5 kHz.

RESULTS

TR-PLI maps obtained for the used photon fluxes are shown in Fig. 1, revealing that lifetime is rather homogeneous, except for small circular areas of lower lifetime and the inscription at the bottom. Note that these are maps of constant *excitation*, representing the sample under typical conditions, e.g. during large area illumination.

For each pixel of a TR-PLI map the injection level can be calculated as follows:

$$\Delta n = \tau_{\text{eff}} \cdot \Phi_{LED} \cdot \frac{(1-R)}{d} \cdot 0.5 \qquad (1)$$

where R is sample reflectivity, d sample thickness and $\Phi_{LED} \cdot 0.5$ the effective photon flux. The factor 0.5 comes about due to the square wave modulated illumination profile used for TR-PLI. Using this, maps of effective lifetime at constant *injection* can be obtained by straightforward pixel by pixel interpolation between the obtained maps, see Fig. 2.

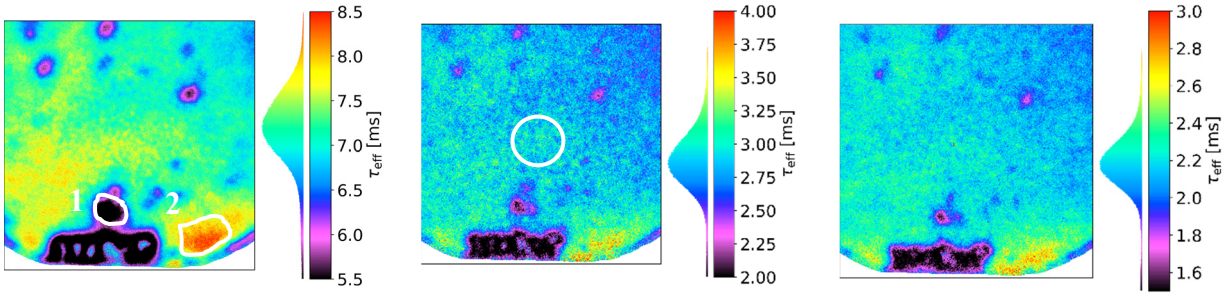

a) b) c)

FIGURE 1. Maps of τ_{eff} from TR-PLI obtained at effective photon fluxes of $1.3 \cdot 10^{16}$ (a), $7.5 \cdot 10^{16}$ (b) and $1.3 \cdot 10^{17}$ $cm^{-2}s^{-1}$(c). Each image has 896x896 data points and shows an area of about 8x8 cm². The inscription is visible near the flat at the bottom. Erroneous data caused by dark noise in the bottom left and right (outside the wafer) has been cropped. Map a) has two areas highlighted with a white outline and map b) shows the location and size of the PCD coil. Note the different scaling for each image.

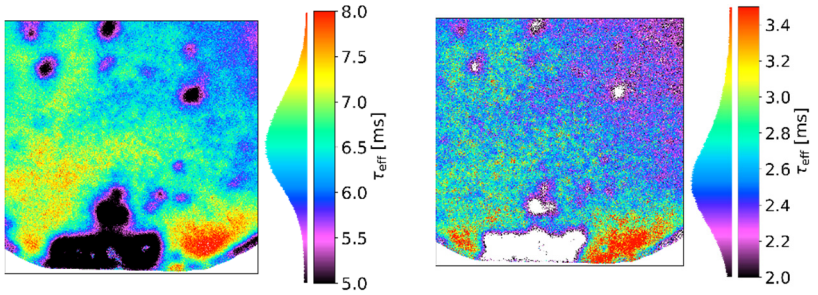

FIGURE 2. Maps of τ_{eff} at constant Δn of $3.5 \cdot 10^{15}$ (a) and $7.5 \cdot 10^{15}$ cm^{-3}(b) obtained from the above images by interpolation. The area outside the wafer has been cropped. Pixels which did not reach the required injection level are displayed as white. Note the different scaling for each image.

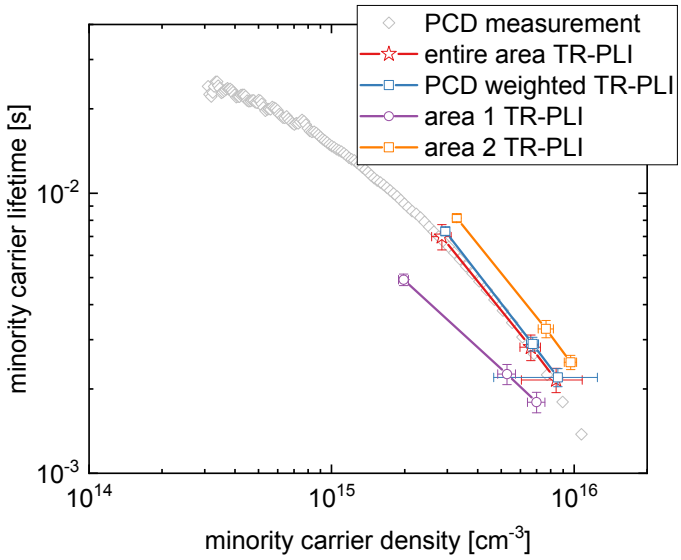

FIGURE 3. Injection dependent minority carrier lifetime, as measured by transient PCD (gray) and by TR-PLI (color). Error bars are standard errors for the respective means. All lines are guides to the eye.

The $\tau(\Delta n)$ curve resulting from the PCD measurement can be seen in Fig. 3 in gray symbols. For each of the maps shown in FIGURE 1, several data points are plotted alongside with the PCD data. Shown in red stars is an average of the entire sample area (excluding off-sample pixels). Blue boxes show the same area, weighted by the PCD coil sensitivity function, as measured by Kiliani et al. [8]. As can be seen, the data points are in close agreement. To illustrate the capability for spatially resolved, injection dependent evaluations, two areas on the sample were selected (c.f. Fig. 1 a), and their averages plotted using purple circles and orange boxes. As expected, area 1 (possibly a point like imperfection in the surface passivation) shows a curve shifted to significantly lower lifetimes. Lifetimes in area 2, on the other hand, are slightly above the PCD values. The average is calculated as the arithmetic average for carrier concentration, and as the harmonic average for lifetimes. Error bars are the respective standard errors of the means.

Numerical Recreation of Experiment

The TR-PLI model relies for its evaluation on the assumption of a lifetime that is independent of injection level. However, this is rarely the case. To obtain meaningful and correct results, it is imperative to choose the right imaging conditions, most importantly the excitation frequency.

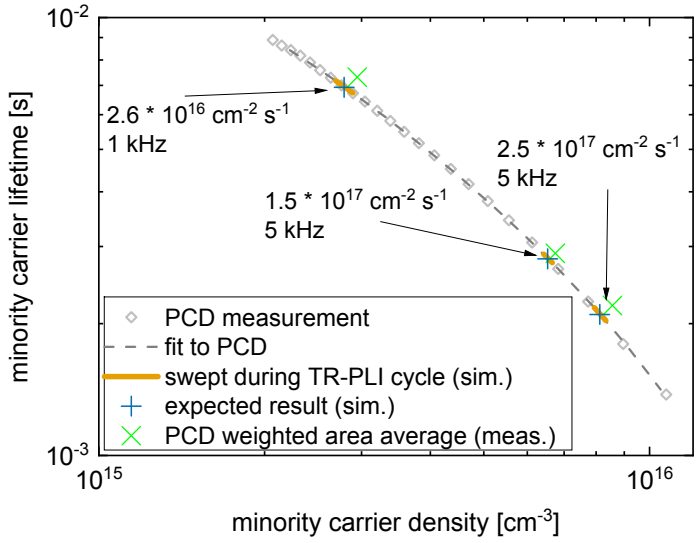

FIGURE 4. Experimental PCD data (light gray) and analytical fit to the data (dark gray, dashed lines). Thick orange strokes show the range of Δn swept during a TR-PLI cycle in the simulation. Blue plus signs show the resulting simulated τ(Δn) point, while green crosses show experimental results.

In this work we used frequencies of 1 kHz (for the lowest light intensity) and 5 kHz, or periods of 1 ms and 0.2 ms respectively. To illustrate whether any effect on the determined lifetime should be expected, the system was simulated: The basic equation

$$\frac{\mathrm{d}\Delta n(t)}{\mathrm{d}t} = G(t) - \frac{\Delta n(t)}{\tau\big(\Delta n(t)\big)} \tag{2}$$

with generation rate G and time t was integrated numerically, with $G(t)$ square wave modulated, and $\tau(\Delta n)$ given by an analytical fit to the experimental PCD data. The fit was used in order to improve the numerical stability of the simulation. Once $\Delta n(t)$ has been determined, the integral

$$\int_{t_1}^{t_2} \Delta n(t) \cdot \big(\Delta n(t) + N_{dop}\big)\, dt \tag{3}$$

for the sliding image integration window of TR-PLI can be calculated (with doping concentration N_{dop}), giving the photoluminescence signal that would be expected from the camera. The obtained (simulated) image intensities can then be fitted in the same way as experimental data to finally give a simulated τ(Δn) data point.

Fig. 4 shows the result of these simulations. The variation in Δn is indeed small, at most 8 % from the mean. Comparison of simulated to experimental values shows a difference of at most 8 %, confirming that imaging conditions were suitable for this sample.

ACKNOWLEDGMENTS

Part of this work was supported by the Federal Ministry for Economic Affairs and Energy on the basis of a decision by the German Bundestag under contract numbers 0324001 and 0324204B. The content is the responsibility of the authors.

REFERENCES

1. R. H. Hopkins and A. Rohatgi, J. Cryst. Growth, **75**, 67-79 (1986).
2. K. Ramspeck, S. Zimmermann, H. Nagel, A. Metz, Y. Gassenbauer, B. Birkmann, and A. Seidl, in *Proc. 27th EUPVSEC* (2012), pp. 861-865.
3. F. Kersten, P. Engelhart, H.-C. Ploigt, A. Stekolnikov, T. Lindner, F. Stenzel, M. Bartzsch, A. Szpeth, K. Petter, J. Heitmann, and J. W. Müller, Sol. Energy Mat. Sol. Cells **142**, 83-86 (2015).
4. D. Chen, M. Kim, B. V. Stefani, B. J. Hallam, M. D. Abbott, C. E. Chan, R. Chen, D. N.R. Payne, N. Nampalli, A. Ciesla, T. H. Fung, K. Kim, and S. R. Wenham, Sol. Energy Mat. Sol. Cells **172**, 293-300 (2017).
5. T. Niewelt, F. Schindler, W. Kwapil, R. Eberle, J. Schön, and M. C. Schubert, Prog. Photovolt. Res. Appl. **26**, 533-542 (2018).
6. N. E. Grant, V. P. Markevich, J. Mullins, A. R. Peaker, F. Rougieux, and D. Macdonald, Phys. Status Solidi Rapid Res. Lett. **10**, 443-447 (2016).
7. W. Kwapil, T. Niewelt, and M. C. Schubert, Sol. Energy Mat. Sol. Cells **173**, 80-84 (2017).
8. D. Kiliani, G. Micard, B. Steuer, B. Raabe, A. Herguth, and G. Hahn, J. Appl. Phys. **110**, 54508 (2011).
9. D. Kiliani, A. Herguth, G. Micard, J. Ebser, and G. Hahn, Sol. Energy Mat. Sol. Cells **106**, 55-59 (2012).
10. R. A. Sinton and A. Cuevas, Appl. Phys. Lett. **69**, 2510-2512 (1996).
11. M. J. Kerr, A. Cuevas, and R. A. Sinton, J. Appl. Phys. **91**, 399-404 (2002).